Preprints (www.preprints.org) | NOT PEER-REVIEWED | Posted: 24 May 2018 doi:10.20944/preprints201805.0343.v1

Article

Surface Plasmon Resonance (SPR) Computational Study of Hemoglobin (Hb) in Human Blood Detection

Wida Yanti [1], Kamsul Abraha [2,*] and Agung Bambang S.U [2]

[1] Departement of Physics, Faculty of Science and Technology, Sunan Kalijaga Islamic State University, Jl Marsda AdiSucipto No.1, Yogyakarta, Indonesia; widayan76@gmail.com
[2] Departement of Physics, Faculty of Mathematic and Natural Science, Gadjah Mada University, Jl Sekip Utara BLS.21, Yogyakarta, Indonesia; kamsul@ugm.ac.id; agungbambang@ugm.ac.id
* Correspondence: kamsul@ugm.ac.id; Tel.: +62-812-271-0165

Abstract: A theoretical analysis of haemoglobin (Hb) concentration detection is presented in this work with the objective of achieving more sensitive detection and monitoring low concentrations. Surface-enhanced SPR spectroscopy on silver nanoparticles was employed for recording Hb concentrations less than 10 g/L. In this paper, Fe_3O_4@Au core-shell, nanocomposite spherical nanoparticle consisting of a spherical Fe_3O_4 core covered by Au shell, was used as an active material for biomolecules detection in the *Surface Plasmon Resonance* (SPR)-based biosensor in the wavelength 632.8 nm. We present the simulation of detection amplification technique through *Attenuated Total Reflection* (ATR) spectrum in the Kretschmann configuration. The system consists of a four-layer material i.e., prism/Ag/Fe_3O_4@Au+Hb/air. Dielectric function determination of the core-shell nanoparticle (Fe_3O_4@Au) and the composite (Fe_3O_4@Au+Hb) was done by applying the *Effective Medium Theory* approximation and the calculation of the reflectivity is carried out by varying the size of core-shell (r_0). In this simulation, the refractive index of the BK7 prism is 1.51; the refractive index of Ag thin film is 0.13455 + 3.98651i with the thickness of 40 nm, and the refractive index of the composite is varied depending on the size of nanoparticle core-shell. Our results show that by varying the radius of the core and the shell thickness, the dip of the reflectivity (ATR) spectrum is shifted to the larger angle of incident light and the addition of core-shell in the conventional SPR-based biosensor leads to enhancement of the SPR biosensor sensitivity, for the core-shell radius 10 nm, the sensitivity increased by 1.35% for F = 0.1, and by 4.89% for F = 0.8 compared to the sensitivity of the conventional SPR-based biosensor without core-shell addition.

Keywords: Haemoglobin detection; SPR spectroscopy; Biosensors; Computer simulation; Core-shell Fe_3O_4@Au.

1. Introduction

Currently, there is increasing interest in the development of magnetic and plasmonic nanoparticles as the active materials for biomolecule detection. The new nanoparticle that combines multiple functions or properties not obtainable in the individual material has attracted considerable attention because of its revolutionary technology for sensitivity enhancement of surface plasmon resonance (SPR)-based biosensor [1]. Optical sensor based on SPR is one of the sensitive methods that detects biomolecules and works on the changes of the material refractive index,

© 2018 by the author(s). Distributed under a Creative Commons CC BY license.

Preprints (www.preprints.org) | NOT PEER-REVIEWED | Posted: 24 May 2018 doi:10.20944/preprints201805.0343.v1

having fast response, real-time, biospecific interaction analysis and being the label-free technique [2]. SPR is a physical process that occurs when the wave vector of the evanescent wave (EW) matches the wave vector of the surface plasmon (SP) under the total internal reflection condition. This resonance condition is expressed as

$$\frac{\omega_0}{c} n_p \sin\theta_{SPR} = \frac{\omega_0}{c}\left(\frac{\varepsilon_m n_d^2}{\varepsilon_m + n_d^2}\right)^{1/2} \tag{1}$$

The variable on left hand side is the propagation constant of a light beam incident at a resonance angle θ_{SPR} through the light coupling device (prism) of refractive index n_p. While the right-hand is the propagation constant with ε_m as real part of the metal permittivity and n_d as the refractive index of dielectric material or sensing medium. ω_0 and c are the light frequency and the speed of the light in the vacuum respectively. The evanescent wave occurs at the metal-dielectric interface when a *p*-polarized wave passes a prism through a metallic layer into a dielectric media.

The wave vector of the evanescent wave is a function of refractive indices of the dielectric, metal and analyte i.e the sensing medium. Therefore, if there is a local change in the refractive index of the sensing medium near the metal surface, it will in turn lead to a change in the propagation constant of SP and in the angle of incidence light in order to satisfy the resonance. For applying SPR biosensor, the Kretschmann geometry [3] of Attenuated Total Reflection (ATR) has been found to be very suitable for the sensing and has become the most widely used geometry in SPR biosensor. Mostly, the metallic layer that is used in SPR biosensor measurement consists of either gold or silver. The first demonstration about SPR-based sensor for bio-sensing was reported in 1983 by Liedberg *et al* [4]. Several ways to enhance sensitivity of SPR biosensor for detecting biomolecules have been explored for the detection of DNA hybridization [5], acetylcholinesterase [6], membrane protein [7] and human blood-group [8]. SPR can also be a potential candidate for bio-sensing other biological properties such as haemoglobin concentration.

From some of researches it is acquired that the conventional SPR-based biosensor was not capable of sensing the small amount biomolecules such as DNA, virus or bacteria [9] due to the poor attachment of biomolecule on the metal surface and the low concentration of it is difficult to detect directly [10]. It happens since the changes in the refractive index of the medium [11] under a thin metal layer are very small. Therefore, the enhancement of sensitivity for detecting small biomolecules can be developed by several approaches such as by involving nanoparticle core-shell as the active material in the conventional SPR-based biosensor. Comparing with nanoparticle which has a spherical shape, the involvement of core-shell aims to avoid polar resonance [12] and to obtain some plasmonic wavelength by varying the radius of the core and the thickness of the shell. A core-shell was said to be a unique material since it is a combination of magnetic and plasmonic materials which has different optical properties between the core and the shell. Some studies have observed, either experimentally or theoretically, about the optical properties of the core-shell with its involvement in the SPR-based biosensor. It is observed that the optical response or resonance spectrum of the core-shell depends on the size of the core and the thickness of the shell. Hence, the

 doi:10.20944/preprints201805.0343.v1

core-shell can be used for tuning the plasmonic wavelength [13], e.g $AgSiO_2$ [12], TiO_2@Au and TiO_2@Ag [14]. The study of the optical response of Fe_3O_4@Au core-shell was performed by varying the radius of Fe_3O_4 and the thickness of Au. There was shift resonance spectrum due to the changes of the size of the core and the shell [15]. The core Fe_3O_4 could make the biomolecule attachment easier by the help of its magnetic property, while the shell Au exhibits nontoxicity and compatible property. Furthermore, the performance of the SPR-based biosensor can be enhanched by using the nanoparticle core-shell Fe_3O_4@Au rather using only Fe_3O_4 or only Au. The presence of Fe_3O_4@Au is also capable of enhancing the immobilization of biomolecules e.g Haemoglobin [16], detecting antibody IgG [17] and detecting the DNA of chum salmon [18].. Whereas, involvement of the Fe_3O_4@Au in the SPR-based biosensor was performed for enhancement detection of thrombin [19], and protein concentration of interleukin IL17 [20]. Detection of the haemoglobin concentration has been explored by SPR-based biosensor for three wavelengths (401.5 nm, 589.3 nm and 706.5 nm) with haemoglobin concentration varying between 0 and 140 g/l [21].

Due to the coating of Au shell for the magnetic core that protected it from oxidation and aggregation, the stabilization of the core-shell (Fe_3O_4@Au) was enhanced *obviously*. And the current SPR technology has so many advantages as well, i.e processing high sensitivity and selectivity, non-destructive, large *tunability* from the visible into the *infrared* (IR) spectrum region, label-free analysis and being capable of real-time monitoring. SPR is a kind of electromagnetic resonance that exists when there is an interface between metal and dielectric. This system has been used for sensing various biomolecules [22],[23]. This method is very sensitive to size, shape and the refractive index of surrounding medium or the medium that kept contact with the thin metal layer. When the biomolecule comes in contact with the metal thin film, it is adsorbed on its surface and hence increasing the refractive index at the interface and resulting in a change of the resonance angle.

In this paper, we have been investigating the ATR spectrum of three and four multilayer biosensor based on SPR system with Fe_3O_4@Au core-shell addition and the biology element is hemoglobin in the human blood with the refractive index is 1.338 [24]. The different size of Fe_3O_4@Au+Hb composites leads to a change in the SPR resonance angle.

This study was focused on the simulation of the effects of the size of the core radius and shell thickness to the effective permittivity of Fe_3O_4@Au. Also, the effects of the volume fraction and the size of the core-shell on the composite effective permittivity and on the SPR-based biosensor reflectivity were investigated. Then, the enhancement of the sensitivity of SPR configuration was estimated.

2. Materials and Methods

2.1. *Kretschmann configuration with four layers*

Here, we apply the analytical and computational approximation to calculate reflectivity in the Attenuated Total Reflection (ATR) method and determine the effective permittivity of the composite (the mixture of Fe_3O_4@Au and Hb embedded in the water). In this study, we used the Kretschmann configuration [3] with four layers. i.e prism/Ag/composite/air shown in Figure 1. The angle θ_i and θ_r are the incident and the reflection angle respectively, k_z is the wave vector component along *z*-axis, and *d* is the thickness of each layer.

Preprints (www.preprints.org) | NOT PEER-REVIEWED | Posted: 24 May 2018 doi:10.20944/preprints201805.0343.v1

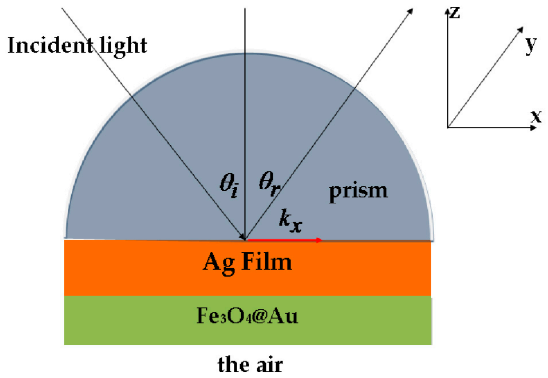

Figure 1. Kretschmann configuration for SPR-based biosensor with the inclusion of Fe_3O_4@Au core-shell.

Figure 2 shows the model of the composite layer containing the inclusion material (Fe_3O_4@Au+biomolecule) and the host material (water). The inclusion material consists of the *scattered grain* material (Fe_3O_4@Au) and the *interfacial shell* material (Hb).

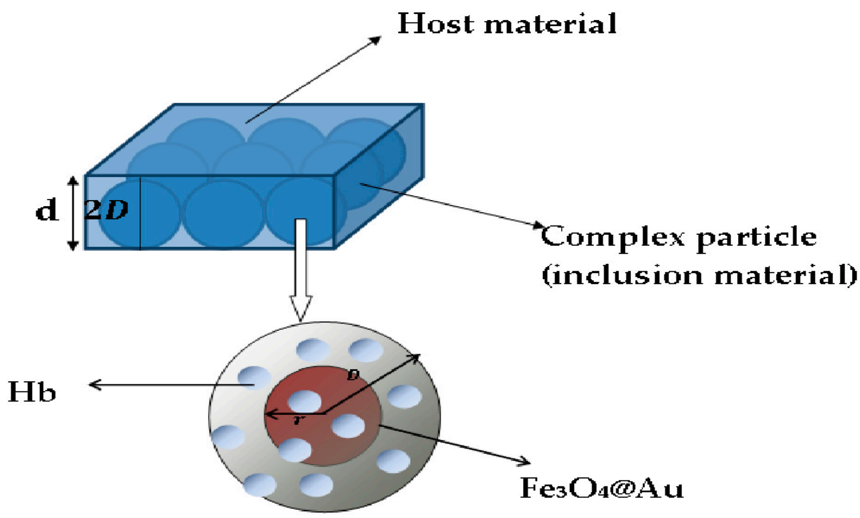

Figure 2. The composite model contains the complex particle (inclusion) and the host material.

In this SPR configuration, the refractive index of the BK7 glass prism is 1.510, the wavelength of the electromagnetic wave is 632.8 nm, the complex refractive index of silver 0.13455+3.98651*i* [25], and dielectric constant of Hb (ε_1) 1.338 for the concentration is less than 10 g/L. The refractive index of water and air is 1.33 and 1.0 respectively [9]. The thickness of Ag film was *d*=40 nm, and the composite was *d*=20 nm. The ATR reflectivity *R* is given by the Fresnel equation [26].

$$R = \left| r_{ijk} \right|^2 = \left| \frac{r_{ij} + r_{jk} e^{2ik_{jz}d_j}}{1 + r_{ij} r_{jk} e^{2ik_{jz}d_j}} \right|^2 \tag{2}$$

with

Preprints (www.preprints.org) | NOT PEER-REVIEWED | Posted: 24 May 2018 doi:10.20944/preprints201805.0343.v1

$$r_{ij} = \frac{k_i \varepsilon_j - k_j \varepsilon_i}{k_i \varepsilon_j + k_j \varepsilon_i} \tag{3}$$

here, r_{ij} is the surface reflectivity coefficient between medium i and medium j. k_{ij} is the wave vector component perpendicular to the surface, k_x is the wave vector component parallel to the surface, whereas d_j and ε_i are respectively the j-th layer thickness and the i-th medium dielectric constant.

2.2. *The effective permittivity of the spherical Fe_3O_4@Au core-shell*

Our simulation of the Fe_3O_4@Au core-shell is performed on the model as shown in Figure 3. The magnetic nanoparticle core-shell consists of a Fe_3O_4 core of radius b coated by a metallic Au of thickness $(a - b)$. The dielectric constants of the magnetic nanoparticle and the metallic Au are ε_c, and ε_s , respectively.

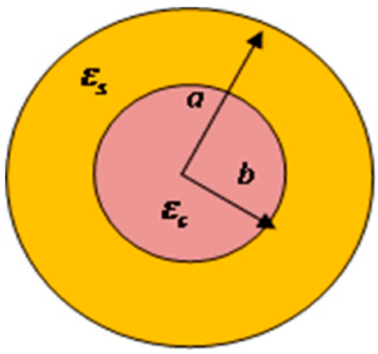

Figure 3. The model of nanoparticle Fe_3O_4@Au core-shell.

whereas, the value of complex ε_c is adopted from Schlegel [27] through reflectivity measurement and Kramers-Kronig relation and ε_s can be quoted from Johnson and Christy work [25]. The effective permittivity $(\varepsilon_{\text{eff}})$ of Fe_3O_4@Au core-shell is derived from the internal homogenization for plasmonic and dielectric constituent material [28], namely

$$\varepsilon_{\text{eff}} = \varepsilon_s \frac{a^3(\varepsilon_c + 2\varepsilon_s) + 2b^3(\varepsilon_c - \varepsilon_s)}{a^3(\varepsilon_c + 2\varepsilon_s) - b^3(\varepsilon_c - \varepsilon_s)} \tag{4}$$

2.3. *Calculating the effective permittivity of the composite*

The effective permittivity of the composite $(\varepsilon_{\text{eff}})$ is calculated by neglecting the correlation between the inclusion material (complex material or Fe_3O_4@Au+Hb) and host material (water), using the Maxwell Garnett formula [29]

$$(1-F)\frac{\varepsilon_{\text{eff}} - \varepsilon_m}{2\varepsilon_{\text{eff}} + \varepsilon_m} + F\left(\frac{\varepsilon_{\text{eff}} - \varepsilon_n}{\varepsilon_{\text{eff}} + \varepsilon_n}\right) \tag{5}$$

with

$$\varepsilon_n = \varepsilon_1 \frac{(2\varepsilon_1+\varepsilon_2)+2\alpha(\varepsilon_2-\varepsilon_1)}{(2\varepsilon_1+\varepsilon_2)-\alpha(\varepsilon_2-\varepsilon_1)} \tag{6}$$

where $\alpha = \left({r_0}/{D} \right)^3$, r_0 the radius of Fe_3O_4, D the radius of the complex particle (Fe_3O_4@Au+Hb), F the volume fraction of the inclusion material to the host material, ε_n the dielectric constant of the complex particle and ε_m the dielectric constant of the host material. ε_1 is the Hb dielectric constant as the *interfacial shell*, while ε_2 is the dielectric constant of *scattered grain* (Fe_3O_4@Au *core-shell*).

2.4. Biosensor sensitivity from ATR spectrum

The calculation of the sensitivity of SPR-based biosensor is written as [30]

$$S = \frac{\Delta\theta_{\mathrm{SPR}}}{\Delta n} \tag{7}$$

where $\Delta\theta_{\mathrm{SPR}}$ is the difference of the SPR angle and Δn is the change in refractive index.

3. Results and Discussion

The changes of the radius of the Fe_3O_4 core and the thickness of the Au shell lead to the change in the effective permittivity of Fe_3O_4@Au core-shell While the change of the inclusion material to host material leads to the change in the effective permittivity of the composite. Therefore, if the complex particle is applied to SPR-based biosensor system, this change leads to the enhancement of the sensitivity of this biosensor. We can show from the reflectivity spectrum that the resonant angle shift to the right.

Table 1. The effective permittivity of Fe_3O_4@Au *core-shell* for the shell thickness variation.

b (nm)	*a* (nm)	*Shell thickness* (nm)	$f = (b/a)^3$	ε_{eff} (real , imag)
10	11	1	0.75	1.0092 , 3.2011
10	13	3	0.46	-2.5021 , 3.0123
10	15	5	0.30	-4.8721 , 2.6948
10	17	7	0.20	-6.4556 , 2.3952
10	20	10	0.13	-7.9297 , 2.0516
10	30	20	0.03	-9.7428 , 1.5407
10	40	30	0.02	-10.212 , 1.3921
10	100	90	0.001	-10.539 , 1.2845

Table 2. The effective permittivity of Fe_3O_4@Au *core-shell* for the core radius variation.

b (nm)	a (nm)	$f = (^{b}/_{a})^3$	ε_{eff} (real , imag)
10	11	0.75	1.0092 , 3.2011
12	13	0.78	1.3637 , 3,2017
14	15	0.81	1.6230 , 3.2000
16	17	0.83	1.8209 , 3.1975
18	19	0.85	1.9768 , 3.1947
20	21	0.86	2.1028 , 3.1921
100	101	0.97	3.0427 , 3.1587

Table 3. The effective permittivity of Fe_3O_4@Au *core-shell* for the $f = (b/a)^3$ variation.

b (nm)	a (nm)	$f = (^{b}/_{a})^3$	ε_{eff} (real , imag)
19	20	0.85	2.04008 , 3.19339
18	20	0.73	0.77837 , 3.19889
17	20	0.61	-0.49070 , 3.16118
16	20	0.51	-1.74550 , 3.08115
15	20	0.42	-2.96636 , 2.96227
14	20	0.34	-4.13333 , 2.81043
13	20	0.27	-5.22780 , 2.63368

Table 1shows the effective permittivity of core-shell (Eq. 4) for variation in the shell thickness. Table 2 shows the effective permittivity of core-shell for variation in the core radius and Table 3 shows the effective permittivity of core-shell for $(^{b}/_{a})^3$ variation. The data in Tabel 1, , Table 2 and Table 3 are presented in Figure 4, Figure 5 and Figure 6 respectively.

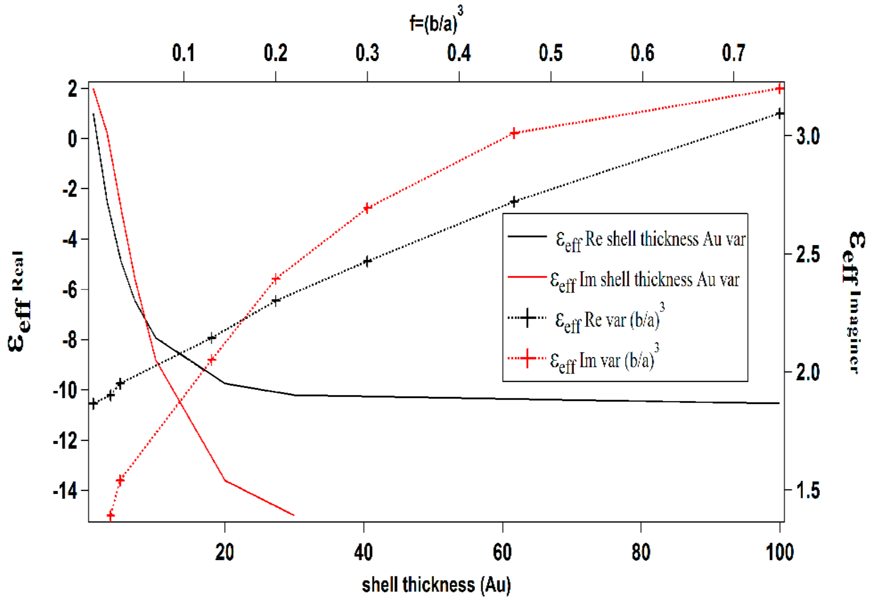

Figure 4. The effective permittivity of *core-shell* for shell thickness variation and $f = (b/a)^3$ variation.

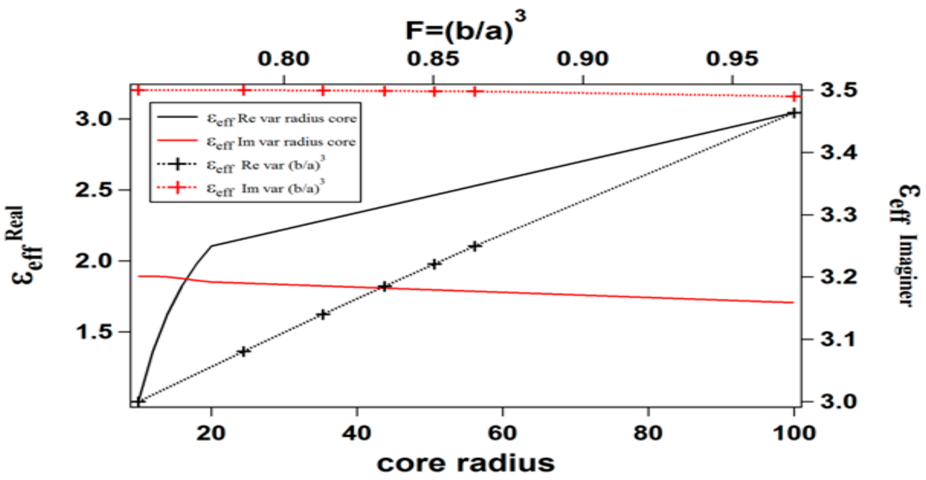

Figure 5. The effective permittivity of *core-shell* for the radius of the core variation and $f = (b/a)^3$ variation.

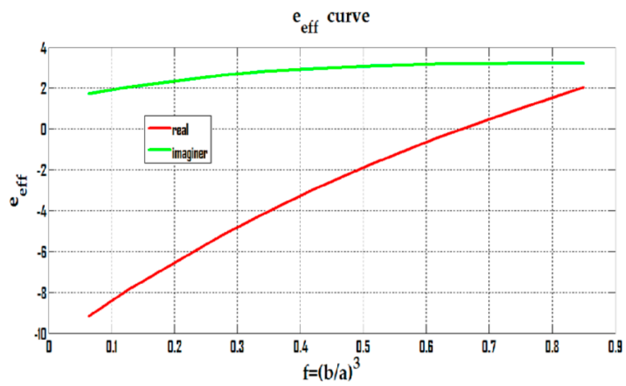

Figure 6. The effective permittivity of *core-shell* for $f = (b/a)^3$ variation.

Figure 4 shows that the increasing shell thickness for fixed core radius (10 nm), leads to the decreasing of the real and imaginary part of the core-shell effective permittivity. But, the real part tends to be constant at the shell thickness above 30 nm. While Figure 5 shows that increasing in the core radius for fixed the shell thickness (1 nm) leads to increasing in the real part of the core-shell effective permittivity while the imaginary part tends to be constant. If the core-shell effective permittivity is viewed only from the $f = (b/a)^3$ variation, it shows that the increasing $f = (b/a)^3$ leads to increasing in the real and imaginary parts of the effective permittivity (Figure 6). Different radius of core-shell a (15 nm, 10 nm, 5nm) with the same $f = (b/a)^3$ variation shows the same effective permittivity value. And then the effective permittivity of the composite can be obtained from Eq. 5.

The thicknesses of Ag metal in this SPR system is the other parameter that must be carefully controlled in order to obtain an optimum performance for surface plasmon excitation. Therefore the choise of the metal thickness is of greatest importance. By varying the Ag thickness, the ATR spectrum shows where the Ag metal film thickness yields the most desirable resonance peak. As the Ag thickness increases (50 -60 nm), the depth of the resonance peak decrease. This is indicate the reduced coupling efficiency of light into the SP mode on the film. This is due to that the metal begins acting as a reflectance plane when its thickness increases to a point where light cannot couple into the surface charge oscillations that make up the plasmon mode. Whereas, if the Ag thin film is very thin (20-30 nm), it result in more coupling into the SP mode but due to light scattering, the sensitivity was redused. Obviously, from these effects, a compromise must be reached to obtain a satisfactory SPR system. Figure 7 was shows the optimal thickness to support SPR system determined to lie at 40 nm.

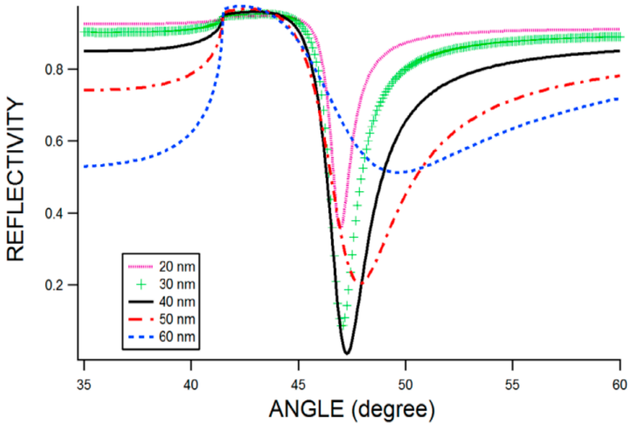

Figure 7. The ATR spectra for the Ag metal thickness varied from 20 nm to the 60 nm.

Based on the above results, we can choose the values of the core radius, the shell thickness and the ratio of the core to the core-shell radius $f = (b/a)^3$to obtain the desirable effective permittivity of the Fe_3O_4@Au core-shell. Figure 8 and Figure 9 shows the effective permittivity of Fe_3O_4@Au+Hb composite (inclusion material) with volume fraction (*F*) variation given by the size variation of the core-shell *a* from 5 nm to 20 nm for fixed $f = (\frac{b}{a})^3 = 0.73$. Here, *F* is the ratio between the amount of the inclusion material to the host material.

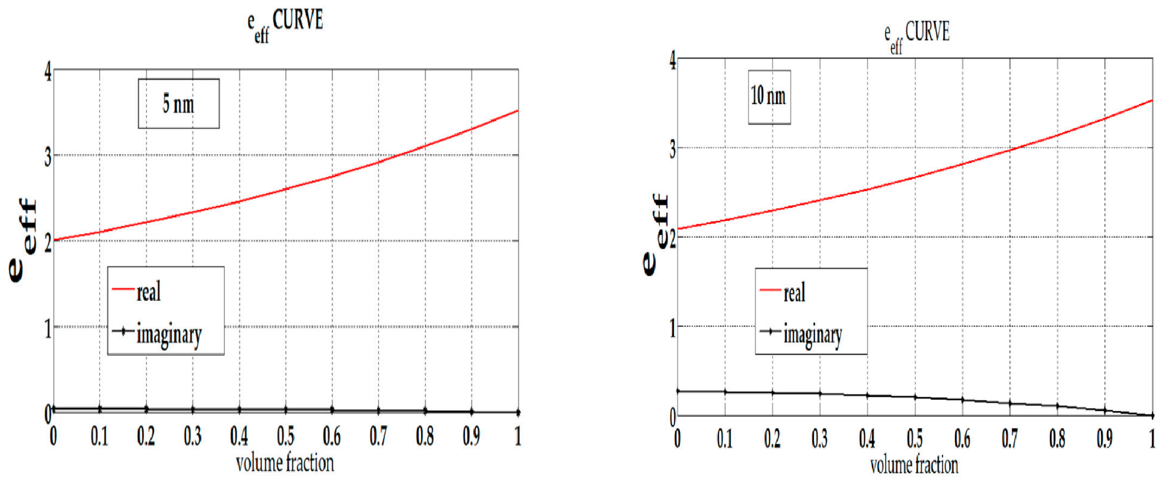

(a) (b)

Figure 8. The composite effective permittivity with variation in the volume fraction (*F*) of composite for fixed size of the core-shell (a) 5 nm (b) 10 nm.

Preprints (www.preprints.org) | NOT PEER-REVIEWED | Posted: 24 May 2018 doi:10.20944/preprints201805.0343.v1

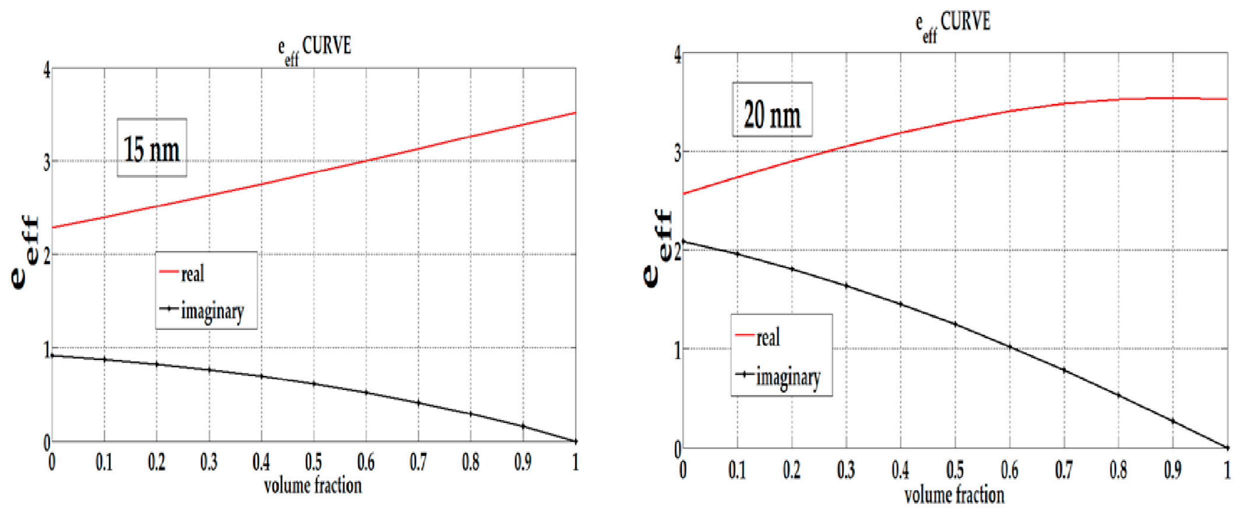

(a) (b)

Figure 9. The composite effective permittivity with variation in the volume fraction (F) of composite for fixed size of the core-shell (a) 15 nm(b) 20 nm.

The reflectivity from the SPR-based biosensor consisting of nanoparticle core-shell is shown in Figure 10 and Figure 11. If the layer only consists of a prism, a thin film of metal (40 nm Ag) and 20 nm biomolecule (conventional SPR), the dip of the ATR curve occurs at the incident angle 45.17^{o} (*solid line*). After the composite had been deposited onto the surface of the Ag thin film, the dip of the reflectivity curve was shifted to the larger angle. Referring to Figure 10 for the volume fraction (F)= 0.1 and the Fe_3O_4@Au radius was varied from 5 nm to 20 nm, the SPR angle was shifted to the larger angle. By increasing the radius of Fe_3O_4@Au, the angle of resonance increases as well. It can be seen in Figure 10 that the minimum reflectivities are seen at 45.75^{o} for thickness 5 nm and at 45.78^{o} for 10 nm thickness, while from Figure 11, for the volume fraction(F)= 0.8 and the Fe_3O_4@Au radius was varied from 5 nm to 20 nm, the SPR angle is shifted to the larger angle as well. The figure shows that the minimum reflectivities occured at 47.38^{o} for thickness 10 nm and at 47.55^{o} for thickness 15 nm.

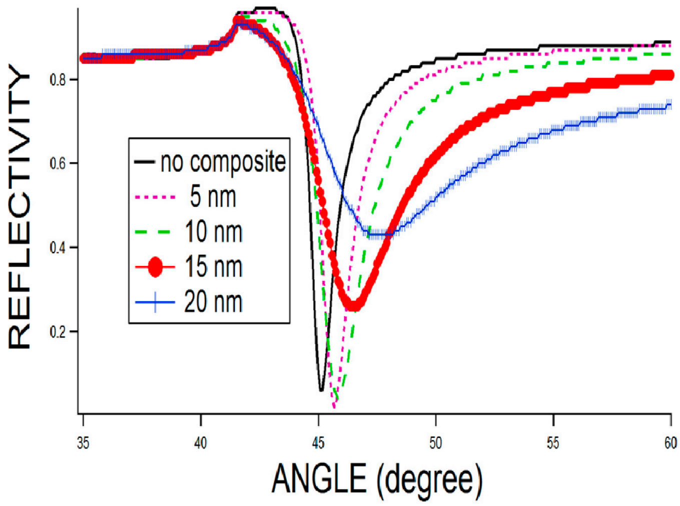

Figure 10. The ATR spectra for the volume fraction of the composite F=0.1. The radius of inclusion material at R=20 nm and the radius of core-shell varied from 5 nm to the 20 nm with fixed $(b/a)^3$=0.73.

Preprints (www.preprints.org) | NOT PEER-REVIEWED | Posted: 24 May 2018 doi:10.20944/preprints201805.0343.v1

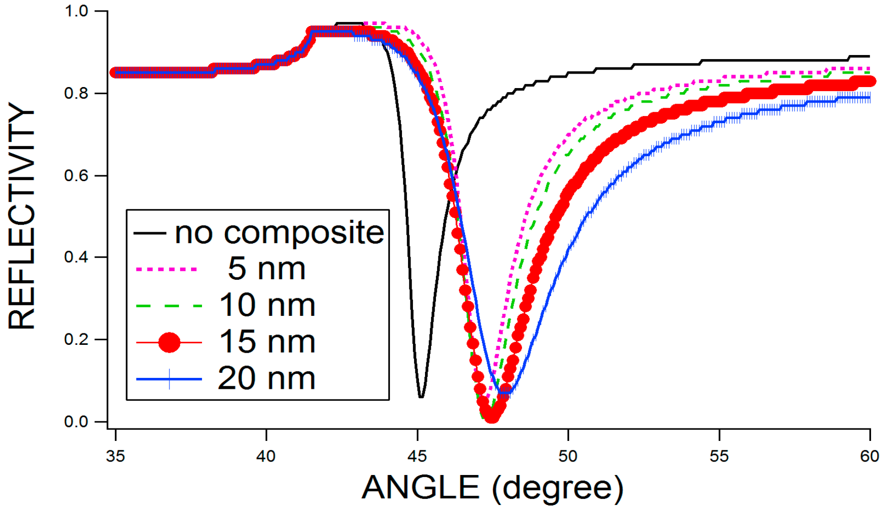

Figure 11. The ATR spectra for the volume fraction of the composite F=0.8. The radius of inclusion material at R=20 nm and the radius of core-shell varied from 5 nm to the 20 nmwith fixed $(b/a)^3$=0.73.

Therefore, it can be obtained from Eq. 7 that for the core-shell radius 10 nm, the sensitivity increased by 1.35 % for F=0.1, and by 4.89 % for F =0.8 compared to the sensitivity of the conventional SPR-based biosensor without core-shell addition

5. Conclusions

In summary, we have presented a simulation for the size effect of the inclusion material in the SPR-based biosensor through the ATR spectra. Our calculations confirm that the property combination of the magnetic and plasmonic materials leads to the enhancement of the SPR-based biosensor sensitivity that applies to detect the existence of Hb as analyte. By varying the radii of the core (Fe_3O_4) and the shell (Au), the refractive index of the core-shell changes and leads to the change in the composite (core-shell+Hb+water) permittivity. The change in this effective permittivity results in the change of the dip position in the reflectivity spectrum to the larger angle. The SPR dips were shifted when the core-shell was added to the composite as the active material. This *large shift* in the *dip* angle suggests the potential for its application in the highly sensitive biosensor, in this case, sensing Hb as the analyte.

Author Contributions: Widayanti conceived the idea for the study, conceptualization, data curation, funding acquisition, methodology, software, visualization and writing original draft of the manuscript. Kamsul Abraha contributed to investigated, validated, writing-review & editing draft of the manuscript and Agung Bambang S.U contribute to helped for supervision and validation. Kamsul Abraha as the corresponding author for this manuscript. All author contributed significant effort to the manuscript preparation.

Conflicts of Interest: The authors declare no conflict of interest.

References

1. Wang, J.; Sun, Y.; Wang, L.; Zhu, X.; Zhang, H.; and Song, D. Surface plasmon resonance biosensor based on Fe3O4/Au nanocomposites. *Colloids and Surfaces B: Biointerfaces.* **2010**, 81, 600-606. https://doi.org/10.1016/j.colsurfb.2010.08.007.

Preprints (www.preprints.org) | NOT PEER-REVIEWED | Posted: 24 May 2018 doi:10.20944/preprints201805.0343.v1

2. Agbor, N.E.; Cresswell, J.P.; Petty, M.C.; and Monkman, A.P. An optical gas sensor based on polyaniline Langmuir-Blodgett films. *Sensors and Actuators B: Chemical*. **1997**, 41, 137-141. https://doi.org/10.1016/S0925-4005(97)80286-9.
3. Kretschmann, E.; Raether, H. Notizen: Radiative Decay of Non Radiative Surface Plasmons Excited by Light.. *Zeitschrift Naturforsh*. **1968**, *23* A, 2135-2136, https://doi.org/10.1515/zna-1968-1247.
4. Liedberg, B.; Nylander, C.; Lunström, I. Surface plasmon resonance for gas detection and biosensing. *Sensors and Actuators*. **1983**, 4, 299-304. https://doi.org/10.1016/0250-6874(83)85036-7.
5. He, L.; Musick, M.D.; Nicewarner, S.R; Salinas, F.G.; Benkovic, S.J.; Natan, M.J.; Keating, C.D. Colloidal Au-Enhanced Surface Plasmon Resonance for Ultrasensitive Detection of DNA Hybridization. *Journal of the American Chemical Society*. **2000,** 122, 9071-9077. https://pubs.acs.org/doi/abs/10.1021/ja001215b.
6. Milkani, E.; Lambert, C.R.; Mc Gimpsey, W.G. Direct detection of acetylcholinesterase inhibitor binding with an enzyme-based surface plasmon resonance sensor. *Anal Biochem*. **2011**, 408, 212-219. https://doi.org/10.1016/j.ab.2010.09.009.
7. Salamon, Z.; Macleod, H.A.; Tollin, G. Surface plasmon resonance spectroscopy as a tool for investigating the biochemical and biophysical properties of membrane protein systems. II: Applications to biological systems. *Biochimica et biophysica acta*. **1997**, 1331, 131-152. https://www.ncbi.nlm.nih.gov/pubmed/9325439..
8. Sharma, A.K. Plasmonic biosensor for detection of hemoglobin concentration in human blood: Design considerations. *Journal of Applied Physics*. **2013**, 114, 044701. https://doi.org/10.1063/1.4816272.
9. Wu, L.; Chu, H.S.; Koh, W.S.; Li, E.P. Highly sensitive graphene biosensors based on surface plasmon resonance. *Opt. Express*. **2010**, 18, 14395-14400. https://doi.org/10.1364/OE.18.014395.
10. Liang, R. P.; Yao, G. H.; Fan, L. X.; Qiu, J. D. Magnetic Fe3O4@Au composite-enhanced surface plasmon resonance for ultrasensitive detection of magnetic nanoparticle-enriched α-fetoprotein. *Anal Chim Acta*. **2012**, 737, 22-28https://doi.org/10.1016/j.aca.2012.05.043.
11. Frasconi, M.; Tortolini, C.; Botrè, F.; Mazzei, F. Multifunctional Au Nanoparticle Dendrimer-Based Surface Plasmon Resonance Biosensor and Its Application for Improved Insulin Detection. *Analytical Chemistry*. **2010**, 82, 7335-7342. https://doi.org/10.1021/ac101319k.
12. Baida, H.; Billaud, P.; Marhaba, S.; Christofilos, D.; Cottancin, E.; Crut, A.; Lermé, J.; Maioli, P.; Pellarin, M..; Broyer, M.; Del Fatti, N.; Vallée, F.; Sánchez-Iglesias, A.; Pastoriza-Santos, I.; Liz-Marzán, L.M. Quantitative Determination of the Size Dependence of Surface Plasmon Resonance Damping in Single Ag@SiO2 Nanoparticles. *Nano Letters*. **2009**, 9, 3463-3469. https://doi.org/10.1021/nl901672b.
13. Zhu, J. Surface Plasmon Resonance from Bimetallic Interface in Au–Ag Core–Shell Structure Nanowires. *Nanoscale Research Letters*. **2009**, 4, 977-981. https://dx.doi.org/10.1007%2Fs11671-009-9344-4.
14. Pathak, N.; Ji, A.; Sharma, R.P. Tunable Properties of Surface Plasmon Resonances: The Influence of Core–Shell Thickness and Dielectric Environment. *Plasmonics*. **2014**, 9,651-657. https://doi.org/10.1007/s11468-014-9677-4.
15. Ahmadi, N.; Poursalehi, R.; and Farshi, M.K.M. The Interparticle Coupling Effect on Plasmon Resonance Properties of Magnetite@Au Magnetoplasmonic Nanoparticles. *Procedia Materials Science*. **2015**, 11, 254-258. https://doi.org/10.1016/j.mspro.2015.11.131.
16. Liu, Y.; Han, T.; Chen, C.; Bao, N.; Yu, C. M.; Gu, H. Y. A novel platform of hemoglobin on core–shell structurally Fe 3O 4@Au nanoparticles and its direct electrochemistry. *Electrochimica Acta*. **2011**, *56*, 3238-3247, https://www.cheric.org/research/tech/periodicals/doi.php?art_seq=915551.

Preprints (www.preprints.org) | NOT PEER-REVIEWED | Posted: 24 May 2018 doi:10.20944/preprints201805.0343.v1

17. Wang, J.; Song, D.; Zhang, H.; Zhang, J;, Jin, Y.; Zhang, H.; Zhou, H.; and Sun, Y. Studies of Fe3O4/Ag/Au composites for immunoassay based on surface plasmon resonance biosensor. *Colloids and surfaces. B, Biointerfaces.* **2013**, 102, 165-170. https://doi.org/10.1016/j.colsurfb.2012.08.040.
18. Zhou, H.; Lee, J.; Park, T.J.; Lee, S.; and Park, J. Ultrasensitive DNA monitoring by Au-Fe3O4 nanocomplex. *Sensors and Actuator B: Chemical.* **2012**, 163, 224-232, http://dx.doi.org/10.1016%2Fj.snb.2012.01.040.
19. Chen, H.; Qi, F.; Zhou, H.; Jia, S.; Gao, Y.; Koh, K.; and Yin, Y. Fe3O4@Au nanoparticles as a means of signal enhancement in surface plasmon resonance spectroscopy for thrombin detection. *Sensor and Actuator B: chemical.* **2015**, *212*, 505-511, https://doi.org/10.1016/j.snb.2015.02.062.
20. Guo, X. Fe3O4@Au nanoparticles enhanced surface plasmon resonance for ultrasensitive immunoassay. *Sensor and Actuator*. **2014**, *205*, 276-280, http://dx.doi.org/10.1016%2Fj.snb.2014.08.055.
21. Sharma, A.K.; Jha, R.; Pattanaik, H. S. Design considerations for surface plasmon resonance based detection of human blood group in near infrared. *Journal of Applied Physics*, **2010**, 107, 034701. https://doi.org/10.1063/1.3298503.
22. Stuart, D.A.; Haes, A.J.; Yonzon, C.R.; Hicks, E.M.; Van Duyne, R.P. Biological applications of localized surface plasmonic phenomenae. *IEE proceedings. Nanobiotechnology*. **2005**, 152, 13-32. doi: 10.1049/ip-nbt:20045012.
23. Jain, P.K.; Huang, X.; El Sayed, I.H.; El-Sayed, M.A. Review of some interesting surface plasmon resonance-enhanced properties of noble metal nanoparticles and their applications to biosystems'. *Plasmonics*. **2007**, 2, 107-118. https://doi.org/10.1007/s11468-007-9031-1.
24. Zhernovaya, O.; Sydoruk, O.; Tuchin, V.; Douplik, A. The refractive index of human hemoglobin in the visible range. *Physics in Medicine and Biology*. **2011**, 56, 4013-4021. https://doi.org/10.1088/0031-9155/56/13/017.
25. Johnson, P.B.; and Christy, R.W. Optical Constants of the Noble Metals. *Physical Review B*. **1972**, 6,. 4370-4379. https://doi.org/10.1103/PhysRevB.6.4370.
26. Rather, H. *Surface Plasmons on Smooth and Rough Surfaces and Gratings*,; Springer-Verlag, Berlin. **1986**, ISBN 978-3-540-47441-8. https://books.google.co.id/books?id=3rsdAQAAMAAJ.
27. Schlegel, A.; Alvarado, S.F.; and Wachter, P. Optical properties of magnetite (Fe_3O_4). *Journal of Physics C: Solid State Physics*. **1979**, 12, 1157-1164. https://doi.org/10.1088/0022-3719/12/6/027.
28. Chettiar, U.K.; Engheta, N. Internal homogenization: Effective permittivity of a coated sphere. *Opt. Express*. **2012**, 20, 22976-22986. https://doi.org/10.1364/OE.20.022976.
29. XUE, Q. Effective-medium theory for two-phase random composites with an interfacial shell. *J. Mater. Sci. Technol*. **2000**, 16, 367-369. http://www.jmst.org/CN/Y2000/V16/I04/367.
30. Verma, R.; Gupta, B.D.; Jha, R. Sensitivity enhancement of a surface plasmon resonance based biomolecules sensor using graphene and silicon layers. Sensors & Actuators: B. Chemical. **2011**, 160, 623-631. https://doi.org/10.1016/j.snb.2011.08.039.